

This is the authors' version of a paper that was later published as:

Frost, Ray and Erickson, Kristy (2005) Raman spectroscopic study of the hydrotalcite desautelsite $\text{Mg}_6\text{Mn}_2\text{CO}_3(\text{OH})_{16}\cdot 4\text{H}_2\text{O}$. *Spectrochimica Acta Part A: Molecular and Biomolecular Spectroscopy* 61(11):2697-2701.

Copyright 2005 Elsevier.

Raman spectroscopic study of the hydrotalcite desautelsite $\text{Mg}_6\text{Mn}_2\text{CO}_3(\text{OH})_{16}\cdot 4\text{H}_2\text{O}$

Ray L. Frost* and Kristy L. Erickson

Inorganic Materials Research Program, School of Physical and Chemical Sciences,
Queensland University of Technology, GPO Box 2434, Brisbane Queensland 4001,
Australia.

Abstract

The structure of the hydrotalcite desautelsite $\text{Mg}_6\text{Mn}_2\text{CO}_3(\text{OH})_{16}\cdot 4\text{H}_2\text{O}$ has been studied by a combination of Raman and infrared spectroscopy. Three intense Raman bands are observed at 1086, 1062 and 1055 cm^{-1} . A model based upon the observation of three CO_3 stretching vibrations is presented. The CO_3 anion may be (a) non-hydrogen bonded (b) hydrogen bonded to the interlayer water and (c) hydrogen bonded to the brucite-like hydroxyl surface. Two intense bands at 3646 and 3608 cm^{-1} are attributed to MgOH and MnOH stretching vibrations. Infrared bands at 3476, 3333, 3165 and 2991 cm^{-1} are assigned to water stretching bands. Raman spectroscopy has proven a powerful tool for the study of hydrotalcite minerals.

Keywords: stichtite, iowaite, desautelsite, takovite, hydrotalcite, Raman spectroscopy

Introduction

Hydrotalcites are natural minerals based upon a brucite structure in which the divalent cation (Mg^{2+}) is replaced with a trivalent cation such as Al^{3+} . This results in a positive surface charge on the brucite-like surface [1-3]. This positive charge must be counterbalanced by negative charges of anions such as CO_3 or SO_4 . This structural arrangement results in the formation of clay-like layers. Hydrotalcites are often termed layered double hydroxides or LDH's. Hydrotalcites are given by the general formula $[\text{M}^{2+}_{1-x}\text{M}^{3+}_x(\text{OH})_2][\text{A}^{n-}]_{x/n}\cdot y\text{H}_2\text{O}$, where M^{2+} and M^{3+} are the di- and trivalent cations in the octahedral positions within the hydroxide layers with x normally between 0.17 and 0.33 [4, 5]. A^{n-} is an exchangeable interlayer anion. In the hydrotalcites reevesite and pyroaurite, the divalent cations are Ni^{2+} and Mg^{2+} respectively with the trivalent cation being Fe^{3+} . In these cases the carbonate anion is the major interlayer counter anion. In the mineral iowaite the anion is chloride. These hydrotalcites are based upon the incorporation of carbonate into the interlayer with expansions of around 8 Å. Normally the hydrotalcite structure based upon takovite (Ni,Al) and hydrotalcite (Mg,Al) has basal spacings of ~8.0 Å where the interlayer anion is carbonate. If the carbonate is replaced by sulphate then the mineral carrboydite is obtained.

* Author to whom correspondence should be addressed (r.frost@qut.edu.au)

Similarly reevesite is the Ni,Fe hydrotalcite with carbonate as the interlayer anion, which when replaced by sulphate the minerals honessite and hydrohonessite are obtained. If the carbonate is replaced with chloride the mineral iowaite is formed. Many variations in compositions have been reported for hydrotalcites. One of the variations in cations comprises desautelsite in which Al is replaced by trivalent Mn. The mineral is known as desautelsite.

EXPERIMENTAL

The Minerals

The mineral desautelsite was obtained from an Australian Museum and also from The Mineral Research Company. The composition of the hydrotalcites was checked by electron probe analyses. The phase composition was checked by X-ray diffraction.

Raman microprobe spectroscopy

The crystals of hydrotalcite mineral was placed and orientated on a polished metal surface on the stage of an Olympus BHSM microscope, which is equipped with 10x and 50x objectives. The microscope is part of a Renishaw 1000 Raman microscope system, which also includes a monochromator, a filter system and a Charge Coupled Device (CCD). Raman spectra were excited by a Spectra-Physics model 127 He-Ne laser (633 nm) at a resolution of 2 cm^{-1} in the range between 100 and 4000 cm^{-1} . Repeated acquisition, using the highest magnification, was accumulated to improve the signal to noise ratio in the spectra. Spectra were calibrated using the 520.5 cm^{-1} line of a silicon wafer. Powers of less than 1 mW at the sample were used to avoid laser induced degradation of the sample [6-8]. Slight defocusing of the laser beam also assists in the preservation of the sample.

Infrared spectroscopy

Infrared spectra were obtained using a Nicolet Nexus 870 FTIR spectrometer with a smart endurance single bounce diamond ATR cell. Spectra over the 4000 to 525 cm^{-1} range were obtained by the co-addition of 64 scans with a resolution of 4 cm^{-1} and a mirror velocity of 0.6329 cm/s . The spectra were transformed using the Kubelka-Munk algorithm to provide spectra for comparison with absorption spectra.

Spectroscopic manipulation such as baseline adjustment, smoothing and normalisation were performed using the Spectracalc software package GRAMS (Galactic Industries Corporation, NH, USA). Band component analysis was undertaken using the Jandel 'Peakfit' software package, which enabled the type of fitting function to be selected and allows specific parameters to be fixed or varied accordingly. Band fitting was done using a Gauss-Lorentz cross-product function with the minimum number of component bands used for the fitting process. The Gauss-Lorentz ratio was maintained at values greater than 0.7 and fitting was undertaken until reproducible results were obtained with squared correlations of R^2 greater than 0.995.

RESULTS AND DISCUSSION

The Raman and infrared spectra of the mineral desautelsite of formula $\text{Mg}_6\text{Mn}_2\text{CO}_3(\text{OH})_{16}\cdot 4\text{H}_2\text{O}$ is shown in Figure 1. The analysis of the spectral data is reported

in Table 1. Both the infrared and Raman spectra show a complex set of overlapping bands. These bands may be attributed to OH stretching vibrations of the MgOH and MnOH units and to water stretching vibrations. The bands at 2882 and 2776 cm^{-1} in the Raman spectrum and at 2991, 2969 and 2871 cm^{-1} in the infrared spectrum are considered to be due to adsorbed organic material on the surface of the mineral. It should be kept in mind the sample is a natural sample and is not treated in any way. One of the differences between the infrared spectrum and the Raman spectrum is the lack of intensity in the 3000 to 3300 cm^{-1} in the Raman spectrum. This is attributed to the difficulty of using Raman spectroscopy to measure water bands as compared with infrared spectroscopy.

In the Raman spectrum two intense bands are observed at 3646 and 3608 cm^{-1} . Two bands of significantly lesser intensity are observed at 3649 and 3596 cm^{-1} in the infrared spectrum. These bands are assigned to MgOH and MnOH stretching vibrations. Three intense bands are observed in the Raman spectrum at 3509, 3409 and 3325 cm^{-1} and are assigned to water stretching bands. Infrared bands are observed at 3476, 3333, 3165 and 2991 cm^{-1} . These bands are also attributed to water stretching vibrations. In brucite type solids, there are tripod units M_3OH with several metals such as M, M', M''. In hydrotalcites such as those based upon Zn and Mg of formula $\text{Mg}_x\text{Zn}_{6-x}\text{Al}_2(\text{OH})_{16}(\text{CO}_3)\cdot 4\text{H}_2\text{O}$, a number of statistical permutations of the M_3OH units are involved. These are Mg_3OH , Zn_3OH , Al_3OH and combinations such as Mg_2ZnOH , Zn_2MgOH , Mg_2AlOH , Al_2MgOH , Al_2ZnOH , Zn_2AlOH , and even MgZnAlOH . These types of units will be distributed according to a probability distribution according to the composition. In this model, a number of assumptions are made, namely that the molecular assembly is random and that no islands or lakes of cations are formed. In the simplest case namely $\text{Mg}_6\text{Mn}_2(\text{OH})_{16}(\text{CO}_3)\cdot 4\text{H}_2\text{O}$ the types of units would be Mg_3OH , Mg_2MnOH , MgMn_2OH and Mn_3OH . In a somewhat oversimplified model, for the $\text{Mg}_6\text{Mn}_2(\text{OH})_{16}(\text{CO}_3)\cdot 4\text{H}_2\text{O}$ hydrotalcite, the most intense bands would be due to the Mg_3OH , Mg_2MnOH and Mn_3OH bands.

The Raman and infrared spectra of the 650 to 1650 cm^{-1} region are shown in Figure 2. Three intense Raman bands are observed at 1086, 1062 and 1055 cm^{-1} . The ratio of the intensity of these bands is 1.55/0.51/2.05 which is 3/1/4. A model for the assignment of these bands can be made based upon these intensities. The band at 1086 cm^{-1} may be assigned to CO_3 units hydrogen bonded to the surface OH units. And the band at 1062 cm^{-1} the CO_3 units hydrogen bonded to the interlayer water whilst the band at 1055 cm^{-1} is attributed to free or non-hydrogen bonded to CO_3 units. These bands are not observed in the infrared spectrum where only a low intensity broad band is observed at 1079 cm^{-1} . In the Raman spectrum two bands are observed at 1349 and 1342 cm^{-1} with a much broader band at 1393 cm^{-1} . In the infrared spectrum a broad band centred at ~1406 cm^{-1} which may be deconvoluted into component bands at 1505, 1449, 1402 and 1387 cm^{-1} . These bands are attributed to the CO_3 antisymmetric stretching vibrations.

In the Raman spectrum a broad band is observed at 872 cm^{-1} . In the infrared spectrum three bands are observed at 873, 867 and 861 cm^{-1} . A reasonable explanation for these bands was given by Kagunya et al., who showed the presence of a band at 698 and 695 cm^{-1} in the Raman spectra of Mg/Al-hydrotalcites with OH^- and CO_3^{2-} as interlayer anion, respectively and assigned this vibration as the $E_{g(T)}$ mode. An intense band is observed at 535 cm^{-1} and is attributed to the ν_2 mode (Figure 3). A second band is observed in the 25 °C Raman spectrum at 560 cm^{-1} and is also attributed to the ν_2 mode. The observation of two bands is indicative of a loss of degeneracy of the C_{3v} symmetry of the CO_3 anion. In the Raman spectra at 25 °C, three bands are observed at 455, 436 and 422 cm^{-1} . These bands are

attributed to the O-Mn-O bending modes. Three bands are also observed at 313, 281 and 254 cm^{-1} . The first two bands may be attributed to MgO and MnO stretching vibrations.

CONCLUSIONS

Hydrotalcites have a unique structure in that the mineral acts like an anionic clay with a ‘giant’ cation whose charge is counterbalanced by multiple anions in the interlayer. Hydrotalcites are normally not easy to measure in terms of Raman spectroscopy because of their small particle size together with their disordered nature. The Raman spectroscopy of the natural hydrotalcites has the benefit that the crystallization has taken place over eons of time and consequently the particles are sufficiently large to be observed using the Raman microscopic technique.

Hydrotalcites containing carbonate anions are readily measured by Raman spectroscopy as the carbonate anion is an intense Raman scatterer and is an anion which is sensitive to its environment.

In this work, the Raman and infrared spectra of the interlayer anion carbonate have been collected. The splitting of the ν_3 , ν_4 and ν_2 modes indicates symmetry lowering. The symmetry lowering must be taken into account through the bonding of carbonate anion to both water and the brucite-like hydroxyl surface. Water plays an essential role in the hydrotalcite structure. The water is strongly hydrogen bonded to both the anion and the hydroxyl surface. Raman spectroscopy has the advantage of water being a very poor scatterer and hence is difficult to observe compared with IR spectroscopy. Thus the cation OH stretching vibrations are more readily observed with Raman spectroscopy.

Acknowledgments

The financial and infra-structure support of the Queensland University of Technology Inorganic Materials Research Program is gratefully acknowledged. The Australian Research Council (ARC) is thanked for funding.

References

- [1]. R. L. Frost, Z. Ding and J. T. Kloprogge, *Can. J. Spectros.* 45 (2000) 96.
- [2]. R. L. Frost, Z. Ding, W. N. Martens, T. E. Johnson and J. T. Kloprogge, *Spectrochimica Acta*, 59A (2003) 321.
- [3]. L. Hickey, J. T. Kloprogge and R. L. Frost, *J. of Mat. Sc.* 35 (2000) 4347.
- [4]. J. T. Kloprogge, D. Wharton, L. Hickey and R. L. Frost, *Am. Mineral.* 87 (2002) 623.
- [5]. V. Rives Editor, *Layered Double Hydroxides: Present and Future*, 2001.
- [6]. W. Martens, R. L. Frost, J. T. Kloprogge and P. A. Williams, *J. Raman Spec.* 34 (2003) 145.
- [7]. R. L. Frost, W. Martens, J. T. Kloprogge and P. A. Williams, *J. Raman Spec.* 33 (2002) 801.
- [8]. R. L. Frost, W. N. Martens and P. A. Williams, *J. Raman Spec.* 33 (2002) 475.

List of Figures

Figure 1 Raman and Infrared spectra of the hydrotalcite desautelsite in the OH stretching region.

Figure 2 Raman and Infrared spectra of the hydrotalcite desautelsite in the 650 to 1650 cm^{-1} region.

Figure 3 Raman spectrum of the hydrotalcite desautelsite in the 150 to 650 cm^{-1} region.

List of Tables

Table 1 Results of the Raman and Infrared spectroscopic analysis of desautelsite

Table 1 Results of the Raman and Infrared spectroscopic analysis of desautelsite

Desautelsite					
Raman			Infrared		
Band Centre (cm⁻¹)	FWHM (cm⁻¹)	Intensity (%)	Band Centre (cm⁻¹)	FWHM (cm⁻¹)	Intensity (%)
3646	· 68	· 2.39	3688	· 23	· 0.37
3608	· 94	· 4.52	3649	· 58	· 0.61
3509	· 169	· 6.10	3596	· 102	· 1.82
3409	· 196	· 11.24	3476	· 215	· 10.01
3325	· 245	· 9.50	3333	· 264	· 9.63
2882	· 59	· 4.25	3165	· 321	· 7.00
2836	· 45	· 0.21	2991	· 606	· 6.09
2776	· 63	· 1.46	2969	· 96	· 0.57
			2871	· 86	· 0.69
			2516	· 42	· 0.50
1676	· 23	· 0.09	1796	· 15	· 0.19
1638	· 39	· 0.56	1631	· 64	· 0.68
1610	· 38	· 0.59	1596	· 37	· 0.42
1579	· 104	· 0.58	1576	· 25	· 0.16
1440	· 35	· 0.16	1505	· 74	· 5.05
1407	· 15	· 0.15	1449	· 76	· 8.73
1393	· 41	· 1.67	1402	· 56	· 7.15
1372	· 12	· 0.06	1387	· 105	· 25.97
1349	· 16	· 1.27	1301	· 154	· 9.22
1342	· 20	· 1.80			
1303	· 57	· 0.51			
1110	· 8	· 0.04	1079	· 27	· 0.45
1086	· 15	· 1.55	1023	· 21	· 0.17
1062	· 10	· 0.51	986	· 61	· 0.49
1055	· 17	· 2.05			
1016	· 24	· 0.15			
			953	· 37	· 0.71
872	· 93	· 0.97	883	· 6	· 0.23
			878	· 6	· 0.37
			873	· 9	· 1.17
			867	· 10	· 0.48
			861	· 13	· 0.31
			850	· 22	· 0.30
			847	· 4	· 0.03
			826	· 26	· 0.08
			773	· 34	· 0.03
			712	· 7	· 0.31
			705	· 10	· 0.03
560	· 43	· 9.41			
535	· 28	· 26.28			
506	· 55	· 4.07			
455	· 28	· 2.16			
436	· 19	· 0.52			

422 · 24 · <i>0.61</i>	
313 · 26 · <i>0.61</i>	
281 · 30 · <i>2.92</i>	
254 · 59 · <i>1.02</i>	

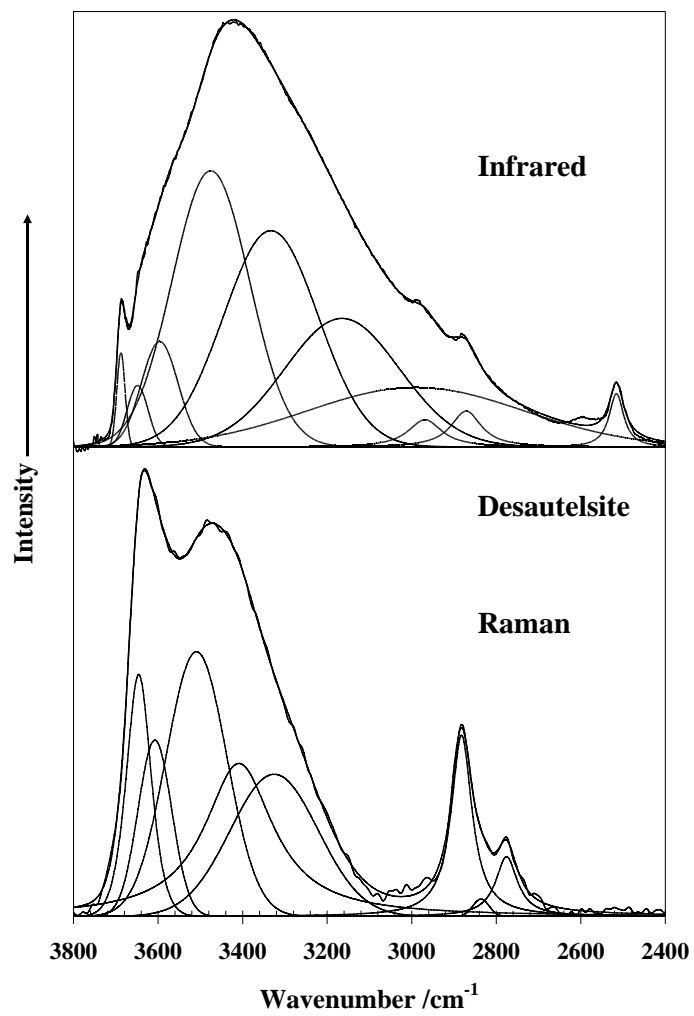


Figure 1

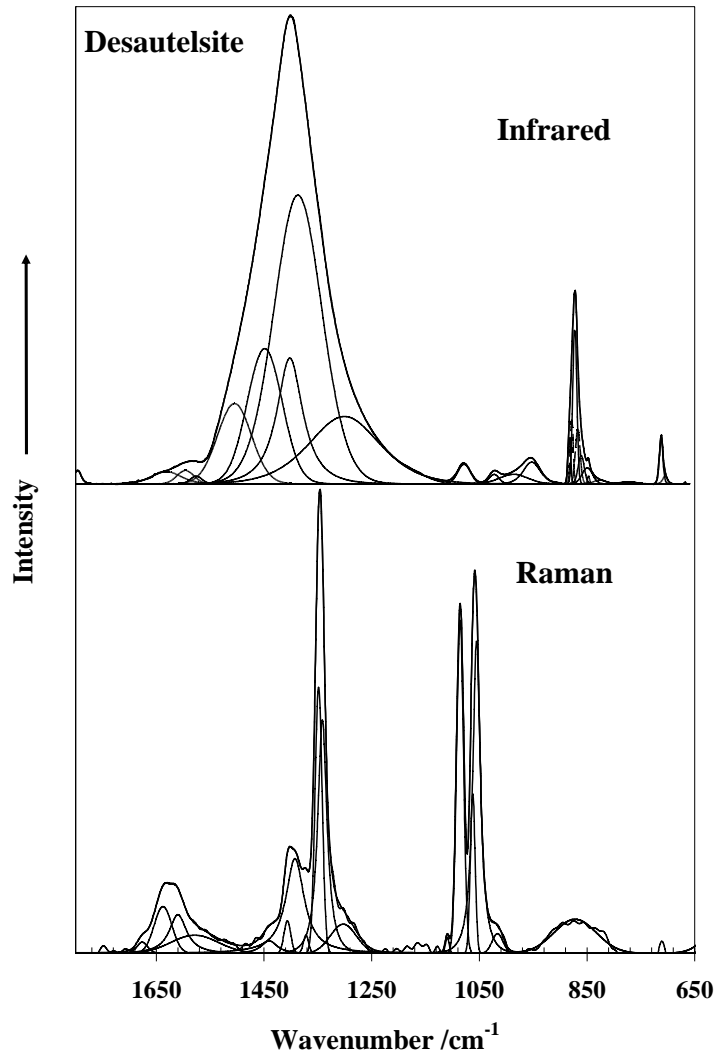


Figure 2

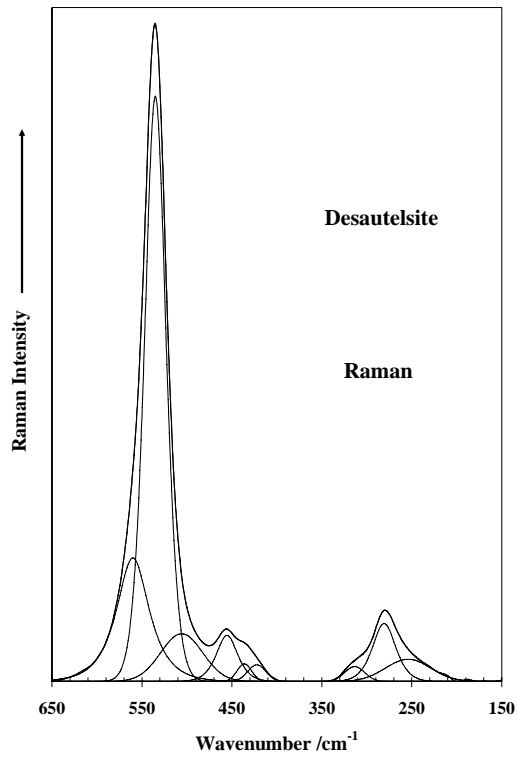


Figure 3

